



---

Year: 2016

---

## Flux Modulations seen by the Muon Veto of the GERDA Experiment

GERDA Collaboration; Agostini, M; Allardt, M; Bakalyarov, A M; et al; Baudis, L; Benato, G; Walter, M

Abstract: The Gerda experiment at Lngs of INFN is equipped with an active muon veto. The main part of the system is a water Cherenkov veto with 66 PMTs in the water tank surrounding the Gerda cryostat. The muon flux recorded by this veto shows a seasonal modulation. Two causes have been identified: ( i ) secondary muons from the Cngs neutrino beam (2.2%) and ( ii ) a temperature modulation of the atmosphere (1.4%). A mean cosmic muon rate of  $I_0 = (3.477 \pm 0.002_{\text{stat}} \pm 0.067_{\text{sys}}) \times 10^{-4} \text{ / (s} \cdot \text{m}^2)$  was found in good agreement with other experiments at Lngs . Combining the present result with those from previous experiments at Lngs the effective temperature coefficient  $T_{\text{Lngs}}$  is determined to  $0.93 \pm 0.03$ . A fit of the temperature coefficients measured at various underground sites yields a kaon to pion ratio  $r_{K/\pi}$  of  $0.10 \pm 0.03$ .

DOI: <https://doi.org/10.1016/j.astropartphys.2016.08.002>

Posted at the Zurich Open Repository and Archive, University of Zurich

ZORA URL: <https://doi.org/10.5167/uzh-129745>

Journal Article

Accepted Version



The following work is licensed under a Creative Commons: Attribution-NonCommercial-NoDerivatives 4.0 International (CC BY-NC-ND 4.0) License.

Originally published at:

GERDA Collaboration; Agostini, M; Allardt, M; Bakalyarov, A M; et al; Baudis, L; Benato, G; Walter, M (2016). Flux Modulations seen by the Muon Veto of the GERDA Experiment. *Astroparticle Physics*, 84:29-35.

DOI: <https://doi.org/10.1016/j.astropartphys.2016.08.002>

# Flux Modulations seen by the Muon Veto of the GERDA Experiment

GERDA collaboration<sup>1,\*</sup>,

M. Agostini<sup>o</sup>, M. Allardt<sup>d</sup>, A.M. Bakalyarov<sup>m</sup>, M. Balata<sup>a</sup>, I. Barabanov<sup>k</sup>, N. Barros<sup>d,8</sup>, L. Baudis<sup>s</sup>, C. Bauer<sup>g</sup>, N. Becerici-Schmidt<sup>n</sup>, E. Bellotti<sup>h,i</sup>, S. Belogurov<sup>l,k</sup>, S.T. Belyaev<sup>m</sup>, G. Benato<sup>s</sup>, A. Bettini<sup>p,q</sup>, L. Bezrukov<sup>k</sup>, T. Bode<sup>o</sup>, D. Borowicz<sup>l,e</sup>, V. Brudanin<sup>e</sup>, R. Brugnera<sup>p,q</sup>, A. Caldwell<sup>m</sup>, C. Cattadori<sup>l</sup>, A. Chernogorov<sup>l</sup>, V. D'Andrea<sup>a</sup>, E.V. Demidova<sup>l</sup>, A. di Vacri<sup>a</sup>, A. Domula<sup>d</sup>, E. Doroshkevich<sup>k</sup>, V. Egorov<sup>e</sup>, R. Falkenstein<sup>r</sup>, O. Fedorova<sup>k</sup>, K. Freund<sup>r</sup>, N. Frodyma<sup>c</sup>, A. Gangapshv<sup>k,g</sup>, A. Garfagnini<sup>p,q</sup>, P. Grabmayr<sup>r</sup>, V. Gurentsov<sup>k</sup>, K. Gusev<sup>m,e,o</sup>, A. Hegai<sup>r</sup>, M. Heisel<sup>g</sup>, S. Hemmer<sup>p,q</sup>, W. Hofmann<sup>g</sup>, M. Hult<sup>f</sup>, L.V. Inzhechik<sup>k,3</sup>, L. Ioannucci<sup>a</sup>, J. Janicskó Csáthy<sup>o</sup>, J. Jochum<sup>r</sup>, M. Junker<sup>a</sup>, V. Kazalov<sup>k</sup>, T. Kihm<sup>g</sup>, I.V. Kirpichnikov<sup>l</sup>, A. Kirsch<sup>g</sup>, A. Klimenko<sup>g,e,4</sup>, M. Knapp<sup>r,5</sup>, K.T. Knöpfle<sup>g</sup>, O. Kochetov<sup>e</sup>, V.N. Kornoukhov<sup>l,k</sup>, V.V. Kuzminov<sup>k</sup>, M. Laubenstein<sup>a</sup>, A. Lazzaro<sup>o</sup>, V.I. Lebedev<sup>m</sup>, B. Lehnert<sup>d</sup>, H.Y. Liao<sup>n</sup>, M. Lindner<sup>g</sup>, I. Lippi<sup>q</sup>, A. Lubashevskiy<sup>g,e</sup>, B. Lubsandorzhiiev<sup>k</sup>, G. Lutter<sup>f</sup>, C. Macolino<sup>a</sup>, B. Majorovits<sup>n</sup>, W. Maneschg<sup>g</sup>, E. Medinaceli<sup>p,q</sup>, M. Misiaszek<sup>c</sup>, P. Moseev<sup>k</sup>, I. Nemchenok<sup>e</sup>, D. Palioselitis<sup>n</sup>, K. Panas<sup>c</sup>, L. Pandola<sup>b</sup>, K. Pelczar<sup>c</sup>, A. Pullia<sup>j</sup>, S. Riboldi<sup>j</sup>, F. Ritter<sup>r</sup>, N. Rumyantseva<sup>e</sup>, C. Sada<sup>p,q</sup>, M. Salathe<sup>g</sup>, C. Schmitt<sup>r</sup>, B. Schneider<sup>d</sup>, S. Schönert<sup>o</sup>, J. Schreiner<sup>g</sup>, A.-K. Schütz<sup>r</sup>, O. Schulz<sup>n</sup>, B. Schwingenheuer<sup>g</sup>, O. Selivanenko<sup>k</sup>, E. Shevchik<sup>e</sup>, M. Shirchenko<sup>m,e</sup>, H. Simgen<sup>g</sup>, A. Smolnikov<sup>g</sup>, L. Stanco<sup>l</sup>, M. Stepaniuk<sup>g</sup>, H. Strecker<sup>g</sup>, L. Vanhoefer<sup>n</sup>, A.A. Vasenko<sup>l</sup>, A. Veresnikova<sup>k</sup>, K. von Sturm<sup>p,q</sup>, V. Wagner<sup>g</sup>, M. Walter<sup>s</sup>, A. Wegmann<sup>g</sup>, T. Wester<sup>d</sup>, H. Wilsenach<sup>d</sup>, M. Wojcik<sup>c</sup>, E. Yanovich<sup>k</sup>, I. Zhitnikov<sup>e</sup>, S.V. Zhukov<sup>m</sup>, D. Zinatulina<sup>e</sup>, K. Zuber<sup>d</sup>, G. Zuzel<sup>c</sup>

<sup>a</sup>INFN Laboratori Nazionali del Gran Sasso, LNGS, and Gran Sasso Science Institute, GSSI, Assergi, Italy

<sup>b</sup>INFN Laboratori Nazionali del Sud, Catania, Italy

<sup>c</sup>Institute of Physics, Jagiellonian University, Cracow, Poland

<sup>d</sup>Institut für Kern- und Teilchenphysik, Technische Universität Dresden, Dresden, Germany

<sup>e</sup>Joint Institute for Nuclear Research, Dubna, Russia

<sup>f</sup>Institute for Reference Materials and Measurements, Geel, Belgium

<sup>g</sup>Max-Planck-Institut für Kernphysik, Heidelberg, Germany

<sup>h</sup>Dipartimento di Fisica, Università Milano Bicocca, Milan, Italy

<sup>i</sup>INFN Milano Bicocca, Milan, Italy

<sup>j</sup>Dipartimento di Fisica, Università degli Studi di Milano e INFN Milano, Milan, Italy

<sup>k</sup>Institute for Nuclear Research of the Russian Academy of Sciences, Moscow, Russia

<sup>l</sup>Institute for Theoretical and Experimental Physics, Moscow, Russia

<sup>m</sup>National Research Centre "Kurchatov Institute", Moscow, Russia

<sup>n</sup>Max-Planck-Institut für Physik, Munich, Germany

<sup>o</sup>Physik Department and Excellence Cluster Universe, Technische Universität München, Munich, Germany

<sup>p</sup>Dipartimento di Fisica e Astronomia dell'Università di Padova, Padova, Italy

<sup>q</sup>INFN Padova, Padova, Italy

<sup>r</sup>Physikalisches Institut, Eberhard-Karls Universität Tübingen, Germany

<sup>s</sup>Physik Institut der Universität Zürich, Zürich, Switzerland

## Abstract

The GERDA experiment at LNGS of INFN is equipped with an active muon veto. The main part of the system is a water Cherenkov veto with 66 PMTs in the water tank surrounding the GERDA cryostat. The muon flux recorded by this veto shows a seasonal modulation. Two effects have been identified which are caused by secondary muons from the CNGS neutrino beam (2.2%) and a temperature modulation of the atmosphere (1.4%). A mean cosmic muon rate of  $I_{\mu}^0 = (3.477 \pm 0.002_{\text{stat}} \pm 0.067_{\text{sys}}) \times 10^{-4} / (\text{s} \cdot \text{m}^2)$  was found in good agreement with other experiments at LNGS at a depth of 3500 meter water equivalent.

**Keywords:** water Cherenkov detector, underground experiment, cosmic rays, muon interaction,

\*Correspondence: gerda-eb@mpi-hd.mpg.de

<sup>1</sup>Laboratori Nazionali del Gran Sasso, Assergi, Italy

<sup>2</sup>present address: maxment GmbH, Germany

<sup>3</sup>also at: Moscow Inst. of Physics and Technology, Moscow, Russia

<sup>4</sup>also at: Int. Univ. for Nature, Society and Man "Dubna",

Dubna, Russia

<sup>5</sup>present address: Areva, France

<sup>6</sup>present address: LAL, Université Paris-Saclay, Orsay, France

<sup>7</sup>present address: Bosch GmbH, Germany

<sup>8</sup>present address: Dept. of Physics and Astronomy, U. of Pennsylvania, Philadelphia, Pennsylvania, USA

## 1. Introduction

The GERDA (**Germanium Detector Array**) experiment is searching for the neutrinoless double-beta decay ( $0\nu\beta\beta$ ) of  $^{76}\text{Ge}$  [1, 2]. It is located in Hall A of the underground laboratory Laboratori Nazionali del Gran Sasso (LNGS) of INFN at a depth of 3500 meter water equivalent (m.w.e.). In order to search effectively for such a rare process as the  $0\nu\beta\beta$  decay GERDA needs to be equipped with a dedicated veto systems which tags muons passing the experiment [1, 3, 4]. Here we report about the observed rates including an annual modulation of the latter during the period 2010–2013 which encompasses Phase I of GERDA. Other underground experiments have observed similar annual modulations of their rates, either due to the muon flux [5] or of other origin [6].

A full explanation of the muon rate is important to assure that the systematics of the experiment are fully understood, in particular when aiming for reduced backgrounds in future phases. A particular problem could be the generation of unstable isotopes by the muons directly or through the secondary neutron flux. Thus, the more obvious sources of backgrounds must be understood. The present results serve also as cross checks to previous or future data sets on muon fluxes in underground laboratories.

## 2. Modulations

The hardware of the muon veto worked very reliable and stable. The overall muon rate of the veto is observed to be modulated by two different sources. Firstly, the majority of the detectable muons are produced cosmogenically [7]. Their spectrum and angular distribution within the halls are both altered by the profile of the rock overburden and have been measured for LNGS with high precision [5]. These muons have an average energy of  $\langle E_\mu \rangle = 270$  GeV. Due to seasonal temperature changes in the atmosphere the mean muon energy changes over the year and thus the muon flux at LNGS.

Secondly, an artificial source for muons was the CERN Neutrinos to Gran Sasso (CNGS) neutrino beam [8] in the period 2008–2012 serving the OPERA experiment [9] for the search of  $\nu_\mu \rightarrow \nu_\tau$  oscillations. This  $\nu_\mu$  beam can create muons by charged current reactions along its 730 km long path. Thus, an additional muon flux is expected during any CNGS beam line operation. As the beam is not operated continuously but pauses in the winter months, the additional flux takes the form of an annual modulation.

Both effects can be described with high precision. The parameters for the atmospheric muon generation are presented in this work which agree well with other experiments at LNGS.

## 3. Instrumentation

The muon veto consists of two parts. The GERDA water tank is instrumented with 66 photomultipliers of 8" size

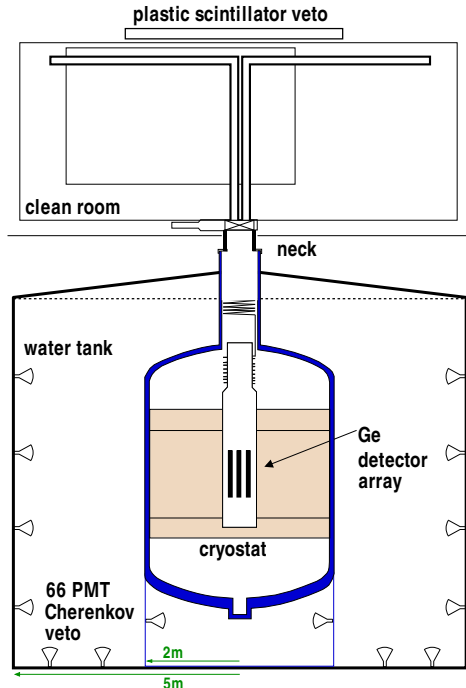


Figure 1: Sketch of the GERDA experiment [1, 3].

which detect the Cherenkov light of passing muons [1, 3] (Fig. 1). The germanium crystals are lowered through the “neck” from the clean room into the liquid argon (LAr) cryostat for normal operation. This “neck” region is less monitored by the Cherenkov veto. Thus, it is covered in addition by a  $4 \times 3$  m<sup>2</sup> layer of plastic scintillators equipped with PMTs on top of the GERDA clean room. In the analysis shown here the standard GERDA muon veto analysis cuts were performed. As described in Ref. [3] a 18 p.e. (photo electron) cut on the Cherenkov data or a valid combination of panels are needed to create a trigger. The stability of the rates and of the light output of veto system was checked periodically.

This muon veto data set contains a period of 806 days from November 2010 to July 2013 that includes also a period before Phase I. Particularly during Phase I of the GERDA experiment the veto system ran continuously stable and reliable.

## 4. Influence of the CNGS beam

The CERN SPS delivered proton bunches with an energy of 400 GeV that hit a carbon target in the CNGS beam line [8]. Actually, each SPS extraction consists of two proton bunches which are 10.5  $\mu\text{s}$  wide and 50 ms apart. Normally, the extraction is repeated every 6 s. Pions and kaons from the collision products are focused on a decay line pointed towards LNGS. These particles can decay according to  $\pi^+/K^+ \rightarrow \mu^+ + \nu_\mu$ . Muon detectors at the end of the decay line record the  $\mu^+$  which can be correlated with the  $\nu_\mu$  intensity. The primary  $\mu^+$  will be

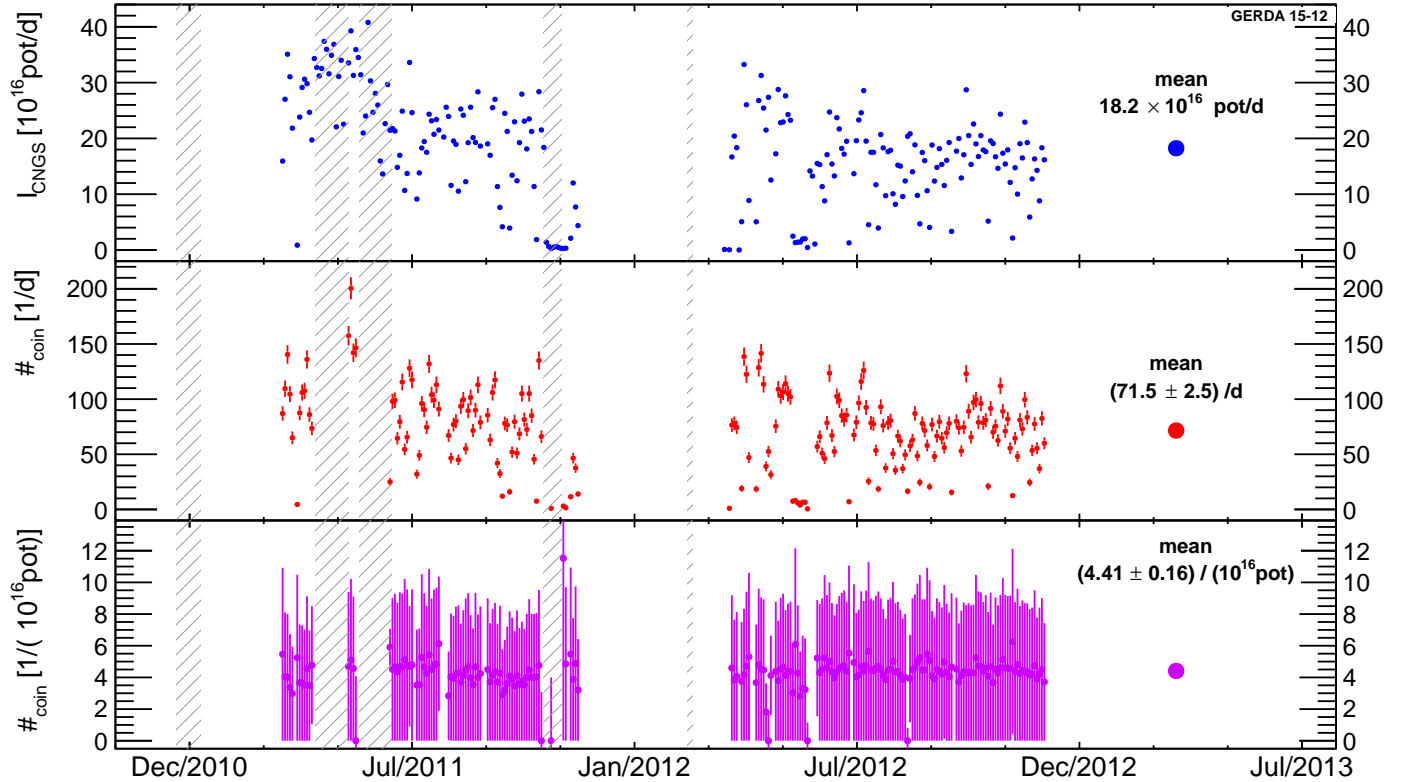


Figure 3: CNGS beam intensities in protons-on-target (POT) and rates over time with a binning of two days. Top: beam intensities measured at CERN; middle: events correlated with the muon veto; bottom: ratio of the two. The grey hatched areas indicate breaks in the muon data-taking.

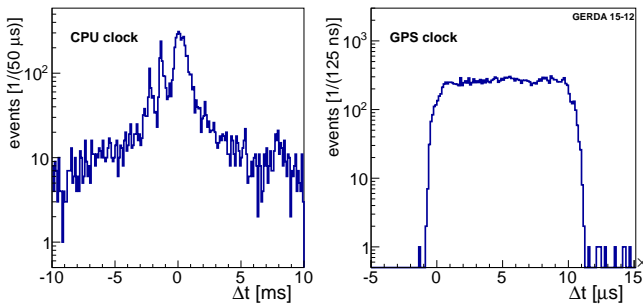


Figure 2: Time offset between CNGS and muon veto events. The left plot shows the time resolution before the installation of the GPS clock, the right one after. The origin in both plots is set to the rising flank of the main feature. Note the different time scales.

stopped on the way towards LNGS while the  $\nu_\mu$  travel almost unhindered. The  $\nu_\mu$  however are able to produce secondary muons of  $\langle E_\mu \rangle = 17$  GeV via  $\nu_\mu + d \rightarrow \mu^- + u$  reactions upstream of LNGS. Thus, an additional muon flux impinges horizontally into the GERDA setup.

Both systems, the CNGS beam at CERN and the muon veto of the GERDA experiment, were operational at the same time during 404 days in 2011 and 2012. In this period  $\sim 28800$  coincident muons due to  $\sim 7 \times 10^{19}$  protons-on-target were detected. The events of both CNGS and muon

veto were correlated by using their respective time stamps. In Fig. 2 the time differences of valid signals from both facilities are shown. The enhancement above the random background shows that true coincidences are observed. In the beginning, the muon veto was running with a CPU clock. However, prior to the start of Phase I a GPS clock was installed [1]. A sharpening of the enhancement of the correlated events is clearly visible from the time spectra of both clock systems. Compared to the CPU clock (Fig. 2, left) the time resolution increased dramatically after the installation of the GPS clock (Fig. 2, right). With the GPS clock the  $10.5 \mu\text{s}$  bunch length of the CNGS beam can be reproduced. This shows that the recorded events can be correlated in time with high accuracy when tested against an external source like the CNGS beam. The accurate timing will also be of advantage when searching for cosmogenic reaction products and their identification via their half life.

In Fig. 3 time series of the daily beam intensities measured at CERN (top), the number of events correlated with the muon veto per day (middle) and the number of coincident events per beam intensity (bottom) are shown. The flat distribution in the bottom panel demonstrates the proportionality between the beam intensity and muon events. This nicely confirms the correct identification of coincident events. The overall fraction of CNGS events in the muon

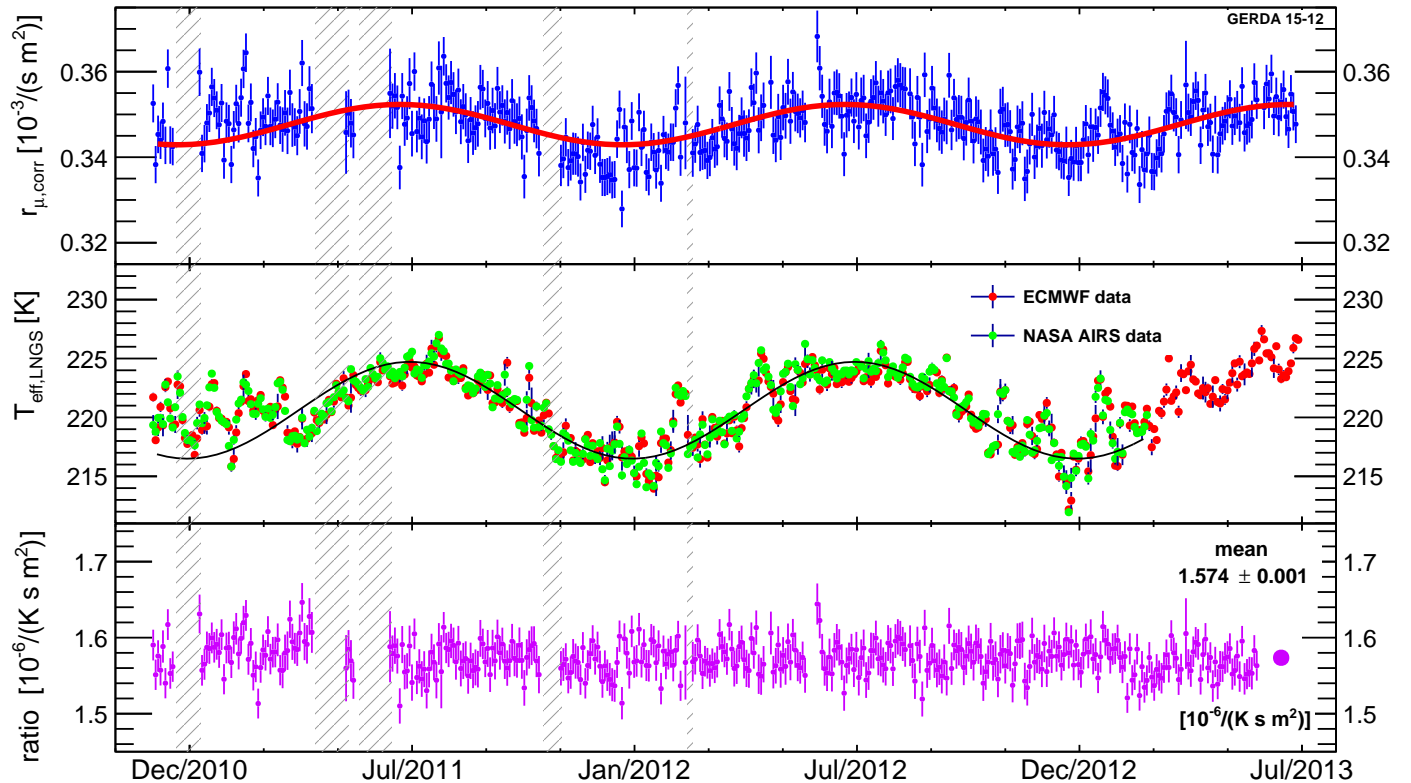


Figure 4: Top: Muon flux measured by GERDA with a binning of two days corrected for the CNGS events. A cosine with a period of 365.25 days is fit to the data. Middle: The effective temperature  $T_{\text{eff}}$  for muon production derived from data of ECWMF [13] in red and from AIRS [14] in green. The black line is a fit to the AIRS data. Bottom: the ratio of the muon rate and the  $T_{\text{eff}}$  from the ECWMF data set is shown to be flat over the entire time.

data is of the order of 2.2%.

Using the time stamps, coincidences between germanium data and CNGS events can be found as well. A number of 45 coincident germanium events were identified in Phase I of GERDA and 42 of these were accompanied by a muon veto trigger and hence correctly discarded. With the rates of the beam and the germanium detectors a number of  $4.9 \pm 2.2$  random coincident events are expected for this period and thus the remaining three germanium events can be attributed to random coincidences.

A single CNGS event was recorded in the 230 keV wide interpolation region around  $Q_{\beta\beta}$  for the background-index (BI) of GERDA. However, this event had a veto flag and was hence excluded from the analysis and had no effect on the BI. Since the CNGS has been decommissioned in 2013, there will be no influence of this type in the next phase of GERDA.

## 5. Atmospheric temperature modulation

The identified events due to the CNGS beam shown in Fig. 3 are removed from the sample for a proper analysis of the temperature dependence of the cosmic muon fraction (see Fig. 4, top). The annual modulation of the muon flux is a well-studied phenomenon [7, 10, 11, 12]. Due to the shielding effect of atmosphere and rock overburden,

only cosmogenically produced muons with an energy above a certain threshold  $E_{\text{thr}}$  will be able to reach an experiment located at a specific depth. Most muons are decay products of pions and kaons in showers caused by cosmic radiation. The amount of energy that can be transferred to their decay products depends on the number of scatterings of the mesons during their life time. The number of scatterings of a meson is governed by its mean free path which depends on the density of the air and ultimately is influenced by the temperature. Hence the atmospheric temperature and the subsequent density of air molecules influence the muon energy spectrum and thus the flux at a certain depth. Since the main temperature change is seasonal, in first order approximation a cosine-like behavior of the flux can be assumed that takes the form

$$I_{\mu}(t) = I_{\mu}^0 + \delta I_{\mu} \cos\left(\frac{2\pi}{T}(t - t_0)\right), \quad (1)$$

where  $I_{\mu}(t)$  is the actual,  $I_{\mu}^0$  the mean muon flux, and  $\delta I_{\mu}$  the amplitude of the modulation;  $t_0$  is the phase marking the summer maximum.

The fit to the rate of the GERDA muon veto is shown in Fig. 4 (top). The period of the fit was fixed to  $T = 365.25$  d because only two maxima are covered up to now. From the top panel it is obvious that a pure cosine-function will not describe the rate modulation due to local weather

conditions changing from year to year, like an unusually warm winter 2010/11. The same kind of deviations can be observed also from the temperature data (Fig 4, middle).

Muon fluxes at LNGS are conventionally given normalized to the effective area of the experiment, i.e. the projection of its geometry on the muon angular spectrum, weighted by the muon intensity. The GERDA water tank has an effective area of  $(103.5 \pm 2.0) \text{ m}^2$ . The fit yields a muon flux of  $I_\mu^0 = (3.477 \pm 0.002_{\text{stat}} \pm 0.067_{\text{sys}}) \times 10^{-4} / (\text{s} \cdot \text{m}^2)$ . The systematic error is derived solely from the uncertainty of the effective area of the water tank. Due to a muon detection efficiency of nearly unity [3] its contributions to the systematic uncertainty becomes negligible. The modulation of  $\delta I_\mu = (4.72 \pm 0.33) \times 10^{-6} / \text{s}$  corresponds to an amplitude of  $(1.4 \pm 0.1_{\text{stat}}) \%$  of  $I_\mu^0$ . The phase  $t_0$  shifts the maximum to the 10<sup>th</sup> of July ( $\pm 4$  days). The fit parameters for the muons agree well with results from other experiments at LNGS, some of them are listed in Tab. 1. The phase of all experiments has its maximum in early July and hence it is not compatible with the phase observed by the DAMA dark matter experiment that is on the 2<sup>nd</sup> of June [6].

The deviation  $\Delta I_\mu(t) = I_\mu(t) - I_\mu^0$  from the detected average muon flux depends on the change in temperature  $\Delta T(X, t)$  of a given layer  $X$  of the atmosphere. The overall change of the muon flux can then be written as an integral over all layers:

$$\Delta I_\mu(t) = \int_0^\infty dX W(X) \Delta T(X, t) \quad (2)$$

The coefficient  $W(X)$  (see Ref. [10] for details) contains both the weight of a certain atmospheric layer to the overall muon flux for both pions and kaons as well as the threshold energy given for a certain underground site, i.e. the rock overburden. The effective temperature  $T_{\text{eff}}$  is a weighted average of the temperature over all layers of the atmosphere assuming the atmosphere to be an isothermal body [10]. It can be approximated as follows:

$$T_{\text{eff}}(t) = \frac{\int_0^\infty dX W(X) T(X, t)}{\int_0^\infty dX W(X)} \quad (3)$$

Similarly for the difference:

$$\Delta T_{\text{eff}}(t) = \frac{\int_0^\infty dX W(X) \Delta T(X, t)}{\int_0^\infty dX W(X)} \quad (4)$$

There are two sets of temperature data available for the period studied. The European Centre for Medium-range Weather Forecast (ECWMF) [13] offers climate data taken by many different observational methods such as weather stations, aircrafts, balloons and satellites to interpolate the climate at any given location. For each location, temperature data for 37 atmospheric pressure levels from 0–1000 hPa are listed four times a day. The second data set is provided by the AIRS instrument [14] on-board the NASA AQUA satellite [15]. The analyses regarding the AIRS data

were produced with data retrieved with the GIOVANNI on-line data system, developed and maintained by the NASA GES DISC [16]. The satellite is in a synchronous orbit with the sun and thus it passes each position of the earth twice per day. The ascending overpass over the Gran Sasso is at about 1:00 a.m. and the descending overpass at 1:00 p.m. AIRS is an infrared sounder and can therefore be disturbed by clouds. Similar to ECWMF it provides temperature data in 24 different pressure levels at any given point. The effective temperature calculated from both datasets can be seen in the middle panel of Fig. 4. Both sets agree very well with their trends and also within their fine-structure despite their different detection and analysis methods. A fit of a cosine-function yields a mean temperature of  $T_{\text{eff}}^{0, \text{AIRS}} = 220.6 \pm 0.2 \text{ K}$  for the AIRS data and  $T_{\text{eff}}^{0, \text{ECWMF}} = 221 \pm 1 \text{ K}$  for the ECWMF data. Both amplitudes are found to be 4 K and the temperature maxima are found on day  $t_0 = 186 \pm 0.5$ , i.e. July 4<sup>th</sup>. Given the short period and the gaps, the agreement between the maxima for the muon rate and for the temperature is more than adequate.

The bottom panel of Fig. 4 gives the ratio of the muon rate and the effective temperature. This ratio is constant for the measured period yielding a mean value of  $(1.57 \pm 0.01) \times 10^{-6} \text{ muons}/(\text{K s m}^2)$ . All the fine structured deviations from the cosine have vanished within the uncertainties.

The change in temperature versus the change in muon flux can be quantified by the Pearson correlation coefficient  $r$ , which is  $+/-1$  for a full positive/negative correlation and 0 for uncorrelated values of  $X = \Delta T_{\text{eff}}(t)/T_{\text{eff}}^0$  and  $Y = \Delta I_\mu(t)/I_\mu^0$ . A graphical representation can be seen in Fig. 5, the coefficients  $r$  of both data sets are around 0.65 and thus a positive linear dependency exists. Therefore, the change in temperature and muon flux can be written as:

$$\frac{\Delta I_\mu(t)}{I_\mu^0} = \alpha_T \frac{\Delta T_{\text{eff}}(t)}{T_{\text{eff}}^0}, \quad (5)$$

where  $\alpha_T$  is an “effective temperature coefficient”. Substituting Eqs. 2 and 4, this coefficient becomes:

$$\alpha_T = \frac{T_{\text{eff}}^0}{I_\mu^0} \int_0^\infty dX W(X). \quad (6)$$

allowing model predictions to access  $\alpha_T$ . Like  $W(X)$ ,  $\alpha_T$  depends on the threshold energy of the respective depth and on the amount of muons from pion and kaon decay. The values derived from linear fits to the two data sets  $\alpha_{T, \text{ECWMF}} = 0.97 \pm 0.05$  and  $\alpha_{T, \text{AIRS}} = 0.93 \pm 0.05$  are in agreement with each other and with the values derived from BOREXINO  $\alpha_{T, \text{bor}} = 0.93 \pm 0.04$  [12] or MACRO  $\alpha_{T, \text{mac}} = 0.91 \pm 0.07$  [18].

This atmospheric model [10, 11, 19, 20] containing both pion and kaon processes can be used to calculate a theoretical value that amounts to  $\alpha_{T, \text{LNGS}} = 0.92 \pm 0.02$  for the LNGS and that agrees well with both experimentally derived values. The values derived from the present fit are

Table 1: List of parameters characterizing the annual modulation of the muon rate according to Ref. [12]. The theoretical value for the effective temperature coefficient for LNGS is  $\alpha_{T,\text{LNGS}} = 0.92 \pm 0.02$ .

experiment	LVD[17]	MACRO[18]	MINOS[11]	BOREXINO[12]	GERDA
site	LNGS-A	LNGS-B	Soudan	LNGS-C	LNGS-A
duty cycle [yr]	8	7	5	4	2.5
published period	2001-08	1991-97	2003-08	2007-11	2010-13
$E_{\text{thr}}$ [TeV] / [km.w.e.]	1.833 / 3.4	1.833 / 3.4	0.73/2.1	1.833 / 3.4	1.833 / 3.4
rate [ $10^{-4}/(\text{s}\cdot\text{m}^2)$ ]	$3.31 \pm 0.03$	$3.22 \pm 0.08$	12.2374(3) Hz	$3.41 \pm 0.01$	$3.47 \pm 0.07$
period [d]	$367 \pm 15$	–	–	$366 \pm 3$	–
phase [d]	$185 \pm 15$	–	–	$179 \pm 6$	$191 \pm 4$
temp. data	Aer.Mil.	Aer.Mil.	ECWMF	ECWMF	ECWMF/AIRS
$T_{\text{eff}}$ model contains	$\pi$	$\pi$	$\pi+K$	$\pi+K$	$\pi+K$
correlation	0.53	0.91	0.90	0.62	0.62/0.65
$\alpha_T$	–	$0.91 \pm 0.07$	$0.879 \pm 0.009$	$0.93 \pm 0.04$	$0.97 \pm 0.05/$ $0.93 \pm 0.05$

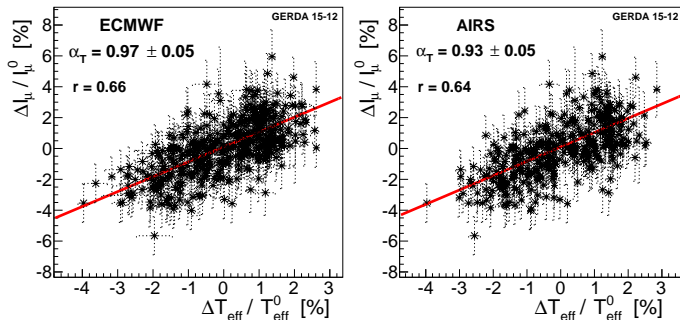


Figure 5: Dependence of the change in muon rate on the change in effective temperature, for both sets of temperature data. A linear fit ( $\chi^2/\text{ndf}_{\text{ECWMF}}=391/410$ ,  $\chi^2/\text{ndf}_{\text{AIRS}}=364/351$ ) yields values for  $\alpha_T$ .

summarized in Tab. 1 and are compared to the results of other experiments at LNGS and Soudan which are in good agreement even though in some analyses atmospheric models which only included muons produced by pion decay are used.

If the amount of rock overburden, i.e. the depth of the laboratory, is varied in the atmospheric model, a relation between depth and  $\alpha_T$  can be calculated [11]. An additional factor in this calculation is the ratio of pions to kaons produced in the atmosphere. Muons which originate from kaons have a higher average energy and are thus less affected by the shielding effect of the rock overburden. A graph of  $\alpha_T$  as a function of depth of observation (Fig. 6) allows for the extraction of the kaon to pion ratio or a comparison of the measurements with the standard ratio. The dotted lines in Fig. 6 show the limits for pure kaon or pure pion decays, i.e.  $r_{K/\pi} = 0$  or  $\infty$ . A model calculation with the literature value for  $r_{K/\pi} = 0.149 \pm 0.06$  [7, 20] (red line) describes all experiments below 500 m.w.e. well.

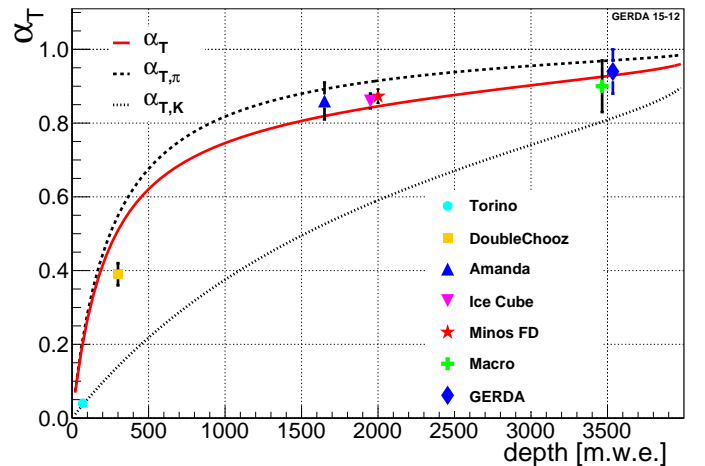


Figure 6: Correlation coefficient  $\alpha_T$  as a function of depth. Experiments with different m.w.e. of rock overburden are listed such as Torino [21], DOUBLE CHOOZ [22], AMANDA [23], ICECUBE [24], MINOS far detector [11], MACRO [18] and GERDA (this work). GERDA and MACRO are located at the same depth but are drawn slightly apart for better visualization. The curves show muon generation models based on either purely pionic (dashed) or only kaonic (dotted) processes. The full red line notes the literature value for the atmospheric kaon/pion ratio [7, 20].

## 6. Summary

The modulation of the muon flux in Hall A of LNGS was identified and quantified using the muon veto data of the GERDA experiment during Phase I and before for a total period of 806 live days.

In these data, two modulation effects with an overall influence on the muon flux of 3–4% could be identified: the additional muon flux caused by the CNGS neutrino beam and the seasonal change in the muon rate caused by temperature variation in the atmosphere which influ-

ences the muon production mechanisms. A clear correlation between the CNGS  $\nu_\mu$  beam and events in the muon veto could be established thanks to the very precise GPS clock in GERDA. These coincident events were subtracted from the data set for further analysis. Coincident CNGS-germanium events were found as well. Most of these events were tagged by the muon veto. The number of untagged events is consistent with the expected number of random coincidences.

An atmospheric model for the seasonal modulation of the muon flux due to atmospheric changes was applied to the data. This model contains both pions and kaons in the muon production mechanism. Two sets of climate data were used to generate an effective temperature, which was found to be in direct relation and in good correlation with the recorded muon flux variation. The results were compared with other experiments and found to be in good agreement as well. A mean muon rate of  $I_\mu^0 = (3.477 \pm 0.002_{\text{stat}} \pm 0.067_{\text{sys}}) \times 10^{-4} /(\text{s}\cdot\text{m}^2)$  was found and the correlation of the modulation with temperature was found to be  $\alpha_{T,\text{ECWMF}} = 0.97 \pm 0.05$  and  $\alpha_{T,\text{AIRS}} = 0.93 \pm 0.05$  for the two data sets of atmospheric data with  $\alpha_{T,\text{LNGS}} = 0.92 \pm 0.02$  being the literature value for LNGS. The atmospheric modulation parameters were compared to other experiments and agree well.

This data set provides a good basis for GERDA Phase II, which aims at 10-fold lower background. The proven good timing will help to identify cosmogenically produced isotopes. Additional analysis of muon data during Phase II of GERDA will allow for more sophisticated analyses including systematic effects.

## Acknowledgments

The GERDA experiment is supported financially by the German Federal Ministry for Education and Research (BMBF), the German Research Foundation (DFG) via the Excellence Cluster Universe, the Italian Istituto Nazionale di Fisica Nucleare (INFN), the Max Planck Society (MPG), the Polish National Science Center (NCN), the Russian Foundation for Basic Research (RFBR), and the Swiss National Science Foundation (SNF). The institutions acknowledge also internal financial support.

The authors would like to thank E. Gschwendter and C. Roderick for providing the CNGS data set and the AIRS and ECWMF groups for providing the climate data used in this work. The authors would also like to thank D. Dietrich and M. Wurm for many helpful discussions and valued input.

## References

[1] K.-H. Ackermann, et al., *Eur. Phys. J. C* **73** (3) (2013) 1.  
 [2] M. Agostini, et al., *Phys. Rev. Lett.* **111** (2013) 122503.  
 [3] K. Freund, et al., submitted to *Eur. Phys. J. C*.  
 [4] K. Freund, Muonic Background in the GERDA  $0\nu\beta\beta$  Experiment, PhD thesis, Universität Tübingen, 2014.

[5] S. Ahlen, et al., *Astrophysical Journal* **412** (1993) 301.  
 [6] R. Bernabei, et al., *Adv. High Energy Phys.* **2014** (2014) 605659.  
 [7] T. Gaisser, *Cosmic Rays and Particle Physics*, Cambridge University Press, 1990.  
 [8] E. Gschwendtner, et al., SS-IEEE06, San Diego, 2006, Report CERN-AB-2007-05 ATB; CERN-ACC-2013-0266 (2013) 4.  
 [9] N. Agafonova et al., *Phys.Lett. B* **691** (2010) 138; *J. of High Energy Physics* **07** (2013) 004.  
 [10] E. W. Grashorn, *Astroparticle physics with the MINOS Far Detector*, Ph.D. thesis, Fermilab (2008).  
 [11] MINOS collaboration, P. Adamson et al., *Phys. Rev. D* **81** (2010) 012001.  
 [12] G. Bellini, et al., *J. of Cosmol. and Astropart. Phys.* **5** (2012) 15.  
 [13] ECWMF, European Centre for Medium-Range Weather Forecasts, <http://www.ecmwf.int/> (2013).  
 [14] NASA, Atmospheric Infrared Sounder (AIRS), <http://airs.jpl.nasa.gov/> (2013).  
 [15] C. Parkinson, Aqua: an earth-observing satellite mission to examine water and other climate variables, *IEEE Transactions on Geoscience and Remote Sensing* **41** (2003) 173. doi: 10.1109/TGRS.2002.808319.  
 [16] J. Acker, G. Leptoukh, *Eos, Trans. AGU* **88** (2007) 14.  
 [17] M. Selvi, *Proc. 31st Int. Cosmic Ray Conf., Lodz* (2009).  
 [18] M. Ambrosio, et al., *Phys. Rev. D* **67** (2003) 042002.  
 [19] E. W. Grashorn et al., *Astropart. Phys.* **33** (2010) 140  
 [20] G. D. Barr, et al., *Phys. Rev. D* **74** (2006) 094009.  
 [21] G. Castagnoli, M. Doderio, *Il Nuovo Cimento B Series* **10** **51** (2) (1967) 525.  
 [22] D. Dietrich, *Studying the muon background component in the Double Chooz experiment*, PhD thesis, Universität Tübingen, 2013.  
 [23] A. Bouchta, *Int. Cosmic Ray Conf.* **2** (1999) 108.  
 [24] P. Desiati, et al., *Proc. 32nd Int. Cosmic Ray Conf., Beijing*, (2011) 78.